EINDHOVEN UNIVERSITY OF TECHNOLOGY

Nitrogen-doping of bulk and nanotubular TiO2 photocatalysts by plasma-assisted atomic layer deposition

Citation for published version (APA):
Zhang, Y., Creatore, M., Ma, Q., El-Boukili, A., Gao, L., Verheijen, M. A., Verhoeven, M. W. G. M., & Hensen, E. J. M. (2015). Nitrogen-doping of bulk and nanotubular TiO2 photocatalysts by plasma-assisted atomic layer deposition. *Applied Surface Science*, *330*, 476-486. https://doi.org/10.1016/j.apsusc.2014.12.197

DOI:
10.1016/j.apsusc.2014.12.197

Document status and date:
Published: 01/01/2015

Document Version:
Publisher's PDF, also known as Version of Record (includes final page, issue and volume numbers)

Please check the document version of this publication:

• A submitted manuscript is the version of the article upon submission and before peer-review. There can be important differences between the submitted version and the official published version of record. People interested in the research are advised to contact the author for the final version of the publication, or visit the DOI to the publisher's website.
• The final author version and the galley proof are versions of the publication after peer review.
• The final published version features the final layout of the paper including the volume, issue and page numbers.

Link to publication

General rights
Copyright and moral rights for the publications made accessible in the public portal are retained by the authors and/or other copyright owners and it is a condition of accessing publications that users recognise and abide by the legal requirements associated with these rights.

• Users may download and print one copy of any publication from the public portal for the purpose of private study or research.
• You may not further distribute the material or use it for any profit-making activity or commercial gain
• You may freely distribute the URL identifying the publication in the public portal.

If the publication is distributed under the terms of Article 25fa of the Dutch Copyright Act, indicated by the "Taverne" license above, please follow below link for the End User Agreement:

www.tue.nl/taverne

Take down policy
If you believe that this document breaches copyright please contact us at:

openaccess@tue.nl

providing details and we will investigate your claim.

Download date: 04. Oct. 2023

Applied Surface Science 330 (2015) 476–486

Contents lists available at ScienceDirect

Applied Surface Science

journal homepage: www.elsevier.com/locate/apsusc

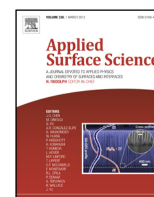

Nitrogen-doping of bulk and nanotubular TiO_2 photocatalysts by plasma-assisted atomic layer deposition

Yi Zhang [a], Mariadriana Creatore [b], Quan-Bao Ma [a], Aishah El Boukili [a], Lu Gao [a], Marcel A. Verheijen [b], M.W.G.M. (Tiny) Verhoeven [a], Emiel. J.M. Hensen [a,*]

[a] Eindhoven University of Technology, Inorganic Materials Chemistry Group, Department of Chemical Engineering and Chemistry, P.O. Box 513, 5600 MB, Eindhoven, The Netherlands

[b] Eindhoven University of Technology, Plasma and Materials Processing Group, Department of Applied Physics, P.O. Box 513, 5600 MB, Eindhoven, The Netherlands

ARTICLE INFO

Article history:
Received 12 August 2014
Received in revised form
16 December 2014
Accepted 31 December 2014
Available online 7 January 2015

Keywords:
Photocatalysis
Titania
Nanotubes
N doping
Plasma-assisted atomic layer deposition

ABSTRACT

Plasma-assisted atomic layer deposition (PA-ALD) was adopted to deposit $TiO_{2-x}N_x$ ultrathin layers on Si wafers, calcined Ti foils and nanotubular TiO_2 arrays. A range of N content and chemical bond configurations were obtained by varying the background gas (O_2 or N_2) during the Ti precursor exposure, while the N_2/H_2-fed inductively coupled plasma exposure time was varied between 2 and 20 s. On calcined Ti foils, a positive effect from N doping on photocurrent density was observed when O_2 was the background gas with a short plasma exposure time (5 and 10 s). This correlates with the presence of interstitial N states in the TiO_2 with a binding energy of 400 eV ($N_{interst}$) as measured by X-ray photoelectron spectroscopy. A longer plasma time or the use of N_2 as background gas results in formation of N state with a binding energy of 396 eV (N_{subst}) and very low photocurrents. These N_{subst} are linked to the presence of Ti^{3+}, which act as detrimental recombination center for photo-generated electron-hole pairs. On contrary, PA-ALD treated nanotubular TiO_2 arrays show no variation of photocurrent density (with respect to the pristine nanotubes) upon different plasma exposure times and when the O_2 recipe was adopted. This is attributed to constant N content in the PA-ALD $TiO_{2-x}N_x$, regardless of the adopted recipe.

© 2015 Elsevier B.V. All rights reserved.

1. Introduction

Titania (TiO_2) has attracted enormous attention in recent decades as a potential material for photocatalytic applications, because it is inexpensive, safe and exhibits high chemical stability [1]. The photocatalytic efficiency of TiO_2 is limited by its large band gap (3.2 eV for the anatase form of TiO_2). One strategy towards improvement of visible light absorption of TiO_2 is the introduction of energy states in the band gap, for instance by cation [2–5] or anion doping [2,6–8]. The former involves doping transition metal ions into the TiO_2 lattice. The metal dopants provide new energy levels as electron donors or acceptors [2]. Typically, anion doping of TiO_2 is preferred over cation doping, because of the introduction of recombination centers in the former case [6]. Anion doping involves introduction of elements such as C, N, S, P or F in the lattice to modify the valence band position [2,6–8]. N is the preferred element, because the atomic radii of N and O are very similar so that N atoms can easily substitute O in the TiO_2 crystal structure [6]. Asahi et al. reported that $TiO_{2-x}N_x$ films can absorb photons with wavelengths longer than 400 nm. These authors also found that the $TiO_{2-x}N_x$ powder has a higher photocatalytic activity towards acetaldehyde decomposition than pure TiO_2 upon visible light excitation [6]. Sato et al. synthesized N-doped TiO_2 by calcination of commercial titanium hydroxide and the resulting material showed higher photocatalytic activity towards oxidation of CO and ethane under visible light than conventional TiO_2 [9]. Livraghi et al. combined experimental and theoretical approaches to investigate the role of N in TiO_2 and reported that the N impurities are responsible for visible light absorption with promotion of charge separation [10].

Compared to bulk films, nanostructured TiO_2 facilitates light harvesting, therefore promoting charge carrier generation as well as their collection at the liquid/solid junction because of the higher surface area [11]. However, the efficiency of three-dimensional nanostructured materials is limited by the relatively poor electron transport through the titania network [12]. One-dimensional nanostructured materials such as nanotubular architectures have been proposed to offer excellent electrons percolation pathways for

* Corresponding author. Tel.: +31 40 247 5178.
E-mail addresses: Y.Zhang2@tue.nl (Y. Zhang), M.Creatore@tue.nl (M. Creatore), Q.Ma1@tue.nl (Q.-B. Ma), AishaBoukili@hotmail.com (A. El Boukili), L.Gao@tue.nl (L. Gao), M.A.Verheijen@tue.nl (M.A. Verheijen), M.W.G.M.Verhoeven@tue.nl (M.W.G.M. Verhoeven), e.j.m.hensen@tue.nl (Emiel.J.M. Hensen).

http://dx.doi.org/10.1016/j.apsusc.2014.12.197
0169-4332/© 2015 Elsevier B.V. All rights reserved.

vectorial charge transfer between interfaces so that the mobility of free electrons is enhanced [13–15].

The influence of N doping on the enhancement of photocatalytic activity was attributed by Asahi et al. to N 2*p*-states, which contribute to the band gap narrowing by mixing with O *2p* states [6]. Many protocols have been developed for N doping of powdered and nanotubular TiO_2, for instance by using N compounds in aqueous solutions containing an appropriate Ti precursor [9,10,16–21], nitridation of TiO_2 in an NH_3 atmosphere, *i.e.* NH_3 treatment [6,22–29], and by combining oxidation and nitridation approaches [30]. In a very recent study, we also investigated nanotubular TiO_2 arrays prepared by anodization and subsequent gaseous NH_3 thermal treatment [28]. It was found that nitridation had a positive effect on the photocurrent density, related to the introduction of interstitial N in the surface. The effect was optimum upon introduction of a very small amount of N, typically 0.4 at%, which was achieved at a NH_3 nitridation temperature of 500 °C. It should be mentioned, however, that it is difficult to control the N content by thermal NH_3 treatment and, typically, only interstitial N can be introduced on the TiO_2 surface. When the temperature of NH_3 treatment is too high, the film becomes fully covered with TiN, resulting in loss of the photocatalytic performance. Also, it has been observed that high temperature nitridation resulted in undesired morphological and textural changes of the nanostructured substrate [28,29]. To minimize such effects, modification of the surface of nanotubular arrays surface with N under milder conditions leading to a tunable content of N are sought.

In order to prepare ultra-thin $TiO_{2-x}N_x$ layers in a more controlled manner in terms of thickness and N content, several groups have employed gas-phase deposition techniques such as chemical vapor deposition (CVD) [31–33], radio-frequency reactive magnetron sputtering [34–36], pulsed laser deposition [37], and, very recently, atomic layer deposition (ALD) [38–40]. In this work, plasma-assisted ALD (PA-ALD) has been explored because it is possible to control the chemical composition, as well as other (*e.g.* opto-electrical, crystallographic and mechanical) properties of the deposited layer [41–43] by tuning the composition of the gas feeding the plasma. Other parameters which contribute to control the properties of the layers are the plasma power, the plasma exposure time and the applied bias at the substrate where deposition occurs [44–49]. As an example, Profijt et al. have shown that the crystal structure of TiO_2 can be tuned from anatase to rutile by varying the bias applied on the substrate holder [45]. Besides, Deng et al. tuned the N content in TiO_2 films by alternating thermal ALD and PA-ALD of TiN [50].

To the best of our knowledge, the deposition of thin $TiO_{2-x}N_x$ layers by PA-ALD on calcined Ti foil and nanotubular TiO_2 arrays has not been reported in literature. In the present study, PA-ALD is applied to develop ultra-thin $TiO_{2-x}N_x$ layers on planar and nanotubular TiO_2 substrates. A systematic study was undertaken to optimize the parameters of the PA-ALD process. For this purpose, the process has been initially investigated on crystalline Si substrates. The nature of the dopant N species and the resulting photo-electrochemical properties of deposited $TiO_{2-x}N_x$/substrate systems are investigated in detail. As a comparison to PA-ALD, NH_3 treatment was also reported on planar TiO_2 substrates. Optimized PA-ALD procedures were then applied to nanotubular TiO_2 substrates and its effect on the photocatalytic properties were investigated.

2. Experimental methods

2.1. Substrates and nanotubular TiO_2 synthesis

Si wafers (CZ Prime, Si(1 0 0) orientation) with diameters of 100 and 200 mm and a 2 nm thick native oxide were purchased from

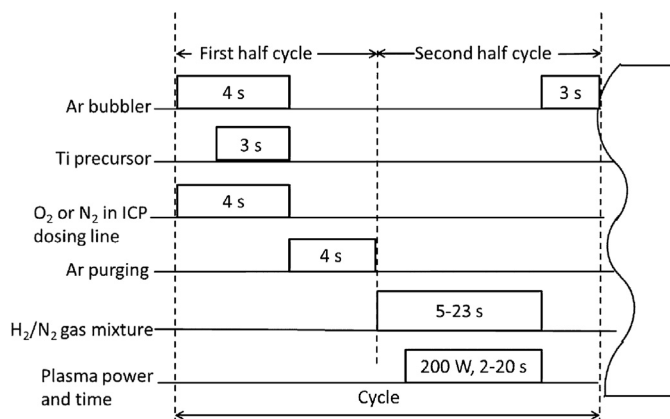

Fig. 1. Flowchart of the PA-ALD process.

Siegert Wafer. The wafers were washed by isopropanol before further use. Ti metal foils were purchased from Advent (>99.6% purity, thickness 0.25 mm). The foils were cut into pieces of 2 cm × 1 cm and then ultrasonically cleaned in acetone, ethanol and distilled water. To develop thin titania films on these foils, they were calcined in a flow oven, under heating with a rate of 5 °C/min to 450 °C and subsequent dwelling for 3 h in artificial air (80/20 v/v ratio of He/O_2). Besides PA-ALD, also thermal nitridation by exposure to NH_3 gas was carried out on these samples. For this purpose, NH_3 gas (NH_3 99.8%, Linde) was led with a flow rate of 200 cm^3/min over the sample, which was placed in a quartz tube in a pipe furnace (Carbolite Type 3508). The nitridation temperature was 500 or 600 °C. The heating rate was 5 °C/min followed by an isothermal dwell of 3 h.

Nanotubular TiO_2 arrays were prepared via electrochemical anodization of a cleaned Ti foil. The Ti foil was immersed in an electrolyte solution containing NH_4F (Merck, >98%) 0.27 M with a volumetric ratio 1:1 of glycerol (Sigma–Aldrich, ≥99.0%) to deionized water at 20 V for 3 h [51]. The as-anodized nanotubular arrays were calcined using the similar procedure as the one discussed for the Ti foil procedure.

2.2. PA-ALD processing

All depositions were carried out in an Oxford Instruments FlexAL^{TM} reactor, which is a load locked remote plasma system with an inductively coupled plasma (ICP) source, placed 31 cm above the substrate holder. The reactor consists of a stainless-steel reaction chamber, which is continuously pumped by a turbo pump for maintaining a base pressure of 10^{-6} mbar. The plasma was generated by a radiofrequency (13.56 MHz) generator with a maximum power of 600 W. The substrate holder with a size of 200 mm was located in the centre of the deposition chamber. The substrate holder could be heated up to 400 °C. For the nitridation procedure as employed here, the used temperatures were 250 °C for the O_2 recipe and 350 °C for the N_2 recipe.

The two ALD half cycles are the exposure of the above-mentioned samples to the Ti precursor, *i.e.* methylcyclopentadiene titanium tris(dimethylamine) [Ti(Cp^{Me})(NMe_2)$_3$] (SAFC Hitech Ltd) [43] and a reactive N_2/H_2-fed ICP generated at a constant power of 400 W. Before deposition, the reactor chamber was pumped to a pressure of 10^{-6} mbar. Fig. 1 reports the O_2 and N_2 recipes for the PA-ALD process. The O_2 recipe started with bubbling Ar for 1 s through the precursor delivery system to enhance the Ti precursor delivery, followed by 3 s exposure of the substrate to the precursor, in a background of O_2 gas injected through the ICP dosing line (gas was injected in the ICP dosing line during the Ti precursor exposure to keep the gas line flushed and prevent any contamination from the outside): the pressure in this first half cycle is constant at

Table 1
Operational parameters for the PA-ALD process.

Recipe	Gas feed (cm^3/min)		Plasma time (s)	Background gases (cm^3/min)			No. cycles	Pressure (mbar)
	N_2	H_2		O_2	N_2	Ar		
O_2	8	60	2,5,10,15,20	50	–	100	250	7×10^{-2}
N_2	8	60	5,15	–	10	100	500	
Combined	8	60	10	50–	–10	100100	60[a]30[a]	

[a] $N_2 + O_2$ cycles repeated for 5 times.

0.13 mbar. This step was followed by a purge with Ar for 4 s. The reactor chamber was preconditioned for 3 s with the gas feed of H_2 and N_2 at a pressure of 7×10^{-2} mbar. Next, the substrate was exposed to the plasma for times ranging from 2 to 20 s. This step was followed by purging the reactor for 3 s. For the N_2 and combined recipes, all process parameters were the same except for the background gases and the number of total cycles (see Table 1).

2.3. Characterization

The morphology of the samples was investigated by Scanning Electron Microscope (SEM, Quanta 3D FEG, FEI) and Transmission Electron Microscopy (TEM, JEM ARM 200). Cross-sectional TEM samples were prepared using Focused Ion Beam (FIB) lift-out preparation. UV–vis absorption spectra were recorded by a Shimadzu UV-2401 PC spectrophotometer in diffusion reflectance mode with $BaSO_4$ as a reference. X-ray diffraction (XRD) patterns were recorded by a Bruker D4 Endeavor diffractometer using Cu Kα radiation. The thickness and refractive index of the samples were determined by means of a Woollam Inc. M2000U Spectroscopic Ellipsometer (SE), ex situ on a goniometric stage as well as in situ during the PA-ALD process. The Si wafer with its SiO_2 native oxide layer were measured by SE before $TiO_{2-x}N_x$ layer deposition to provide a good base for fitting. For the fitting of the SE data of PA-ALD on Si wafer, an optical model (Complete-EASE software) consisting of the Si substrate, the SiO_2 native oxide layer (ca. 2 nm) and the deposited $TiO_{2-x}N_x$ layer was used. Both SiO_2 layer and the deposited $TiO_{2-x}N_x$ layer were modelled with the Cauchy dispersion formula. The surface composition and oxidation states of the constituent elements were determined by X-ray Photoelectron Spectroscopy (XPS). XP spectra were taken using a Thermo Scientific K-Alpha spectrometer with monochromatic Al Kα sources. Spectra were recorded at normal emission background pressure of 1×10^{-8} mbar and all the binding energies were corrected with respect to the reference peak, *i.e.* the C 1s peak at 284.5 eV of adventitious carbon. Depth profiling was carried out by applying an Ar ion beam sputtering with ion energy of 500 eV. For the Si wafer, the surface was sputtered 15 times, with a constant sputter time of 30 s. For the Ti foils and nanotubular TiO_2 arrays, 4 short sputtering cycles of 30 s each were employed followed by 20 longer sputtering cycles of 180 s.

Photoelectrochemical activity measurements were performed in a 3-electrode cell using 0.1 M Na_2SO_4 as the electrolyte solution with a Pt ring counter electrode, a saturated calomel electrode (SCE) as the reference electrode and the (surface modified) TiO_2 as the working electrode. A Xe arc lamp (Oriel Instruments) was used as the light source with a power supply of 200–500 W. The irradiation power in this study was set at 300 W. The photocurrents were reported after subtraction of the dark current.

3. Results and discussion

3.1. PA-ALD on Si wafers

The layer characterization was first carried out on crystalline Si substrates. As an example, Fig. 2 shows the XPS depth profiles for the PA-ALD deposited layer using the O_2 and N_2 recipes with different plasma exposure times as a function of the sputtering time. The thickness of the deposited layer, the composition at the surface and the composition averaged for the whole layer thickness for the O_2, N_2 and combined recipes are collected in Table 2. For the O_2 recipe, the O/Ti ratio at the surface is close to 2 and remains constant as a function of the depth up to a sputtering time of 200 s, corresponding to the depth at which the TiO_2/Si interface is reached. The thickness of the deposited $TiO_{2-x}N_x$ layer as determined by SE is 17.3 ± 1.6 nm. The growth per cycle (GPC) is 0.07 nm/cycle, in agreement with the value reported by Profijt et al. [41]. The N content remains <1 at% at the surface and in the bulk, suggesting that the source of N in the layer is only the N in the precursor molecule. Table 2 shows that the surface N content in $TiO_{2-x}N_x$ layer increases with increasing the plasma exposure time.

Using the N_2 recipe, a $TiO_{2-x}N_x$ layer is deposited with higher N content. This can be primarily attributed to the presence of adsorbed N_2 on the walls of the ICP tube, upon N_2 flushing of the ICP dosing line and subsequent plasma ignition. The average N content with a plasma exposure time of 5 s is approximately 10 at% at the surface. The thickness of this layer measured with SE is 17.0 ± 3.0 nm, which is similar to the layer thickness obtained using the O_2 recipe. The GPC is 0.034 nm/cycle, a factor two lower than found for the O_2 recipe. From the sputtering profile (Fig. 2 (c)), it follows that for the $TiO_{2-x}N_x$ layer with higher N content a shorter etching time was required to reach the interface between PA-ALD layer and substrate than the one with low N content (prepared by the O_2 recipe). As the thicknesses of the two layers are similar, this suggests that the material density of $TiO_{2-x}N_x$ layer with higher N content is lower than that of the one with low N content prepared by the O_2 recipe. The combined recipe results in an average N content of 9 at%. The N content at the surface is around 5 at%. Table 2 also shows that films developed under N_2 and combined recipes contain carbon in the bulk, which most likely derives from incomplete combustion of the organic fragments originating from the organometallic Ti precursor. Fig. 2 shows that the C content at the surface region is typically higher than in the bulk, in agreement with the presence of surface contamination.

Fig. 3 shows the N 1s XP spectra of the films deposited by various recipes. For the films deposited using the O_2 recipe the N content is low for all plasma exposure times. The N content increases with the plasma exposure time as evidenced by the increasing intensity of the weak feature around 400 eV. A plasma exposure time of 20 s leads to appearance of an additional feature at lower binding energy. For the $TiO_{2-x}N_x$ layer deposited with the N_2 recipe, the feature around 396 eV is the dominant one in the XP spectrum and a shoulder at 400 eV is also visible. The peak at 396 eV is also visible in the XP spectrum of the film deposited by the combined recipe, albeit with lower intensity.

Results of the deconvolution of these XP spectra are given in Table 3. The N 1s feature with a binding energy around 400 eV can be assigned to chemisorbed molecules as N_2 [6,24,26,52], nitrogen oxides such as NO_x [18,32,53] or interstitial N. As discussed earlier [28], the most likely origin of this N feature is that of interstitial N, denoted here as $N_{interst}$. Theoretical calculations [54] examined

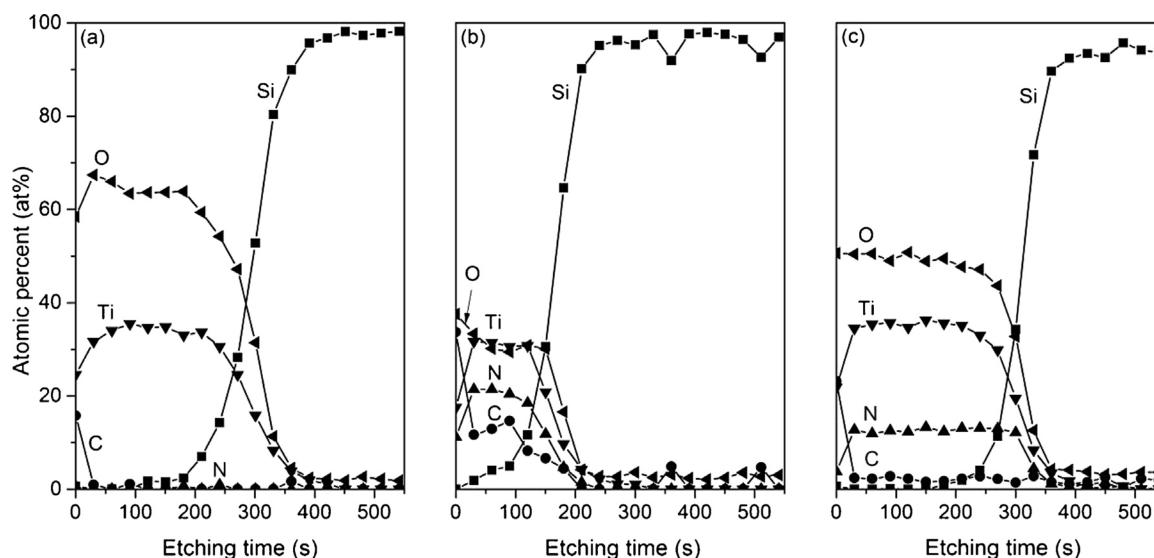

Fig. 2. Concentration profiles of the $TiO_{2-x}N_x$ thin layer prepared by PA-ALD on Si wafers using (a) the O_2 recipe with plasma time of 5 s, (b) the N_2 recipe with plasma time of 5 s and (c) the combined recipe with plasma time of 10 s.

Table 2
Surface and bulk composition of PA-ALD $TiO_{2-x}N_x$ layers on various substrates.

Substrate	Recipe	Plasma exposure time (s)	Layer thickness (nm)	Film composition (at%)				
				Ti	O	Si	N	C
Si wafer	O_2	2	15.2	31[a] (27)[b]	61 (61)	1.5 (0)	0.3 (0.3)	5.9 (12)
		5	17.0	31 (25)	60 (58)	2.5 (0.6)	0.2 (0.3)	5.6 (16)
		10	17.8	29 (25)	64 (60)	0 (0)	0.2 (0.6)	5.7 (14)
		15	17.8	30 (24)	63 (58)	1.2 (0)	0.6 (0.7)	5.7 (17)
		20	18.5	30 (25)	63 (60)	1.5 (0)	1.1 (1.1)	4.7 (14)
	N_2	5	14.8	27 (18)	34 (38)	2.0 (0)	18 (11)	19 (33)
		15	18.3	27 (19)	33 (37)	0.8 (0)	22 (13)	16 (31)
	Combined	10	17.2	32 (26)	50 (48)	0 (0)	9.3 (5.4)	8.1 (21)
TiO_2/ Ti foil	O_2	pristine	–	29 (20)	63 (60)	–	0.8 (0.7)	7.2 (19)
		2	18	28 (19)	61 (55)	–	0.7 (0.8)	9.8 (25)
		5	–	– (25)	– (58)	–	– (1.3)	– (14)
		10		25 (18)	68 (67)	–	0.8 (1.1)	6.0 (14)
		20		34 (25)	62 (61)		0.6 (1.1)	3.5 (13)
	N_2	5	16	27 (11)	36 (33)	–	5.3 (7.4)	31 (49)
		15	–	– (26)	– (44)	–	– (13)	– (17)
	Combined	10	18	31 (22)	51 (49)	–	3.0 (4.6)	15 (24)
TiO_2 Nanotubes	O_2	Pristine	–	27 (23)	62 (56)	–	0.5 (0.8)	11 (20)
		2		27 (23)	62 (57)	–	0.3 (0.6)	10 (19)
		5		28 (24)	64 (60)	–	0.5 (0.9)	18 (15)
		10		33 (30)	61 (59)	–	0.5 (0.7)	5.4 (9.9)
		20		27 (23)	61 (56)	–	0.4 (0.4)	12 (21)
	N_2	5	–	25 (20)	41 (43)	–	14 (7.4)	20 (29)
	Combined	10	–	27 (19)	52 (54)	–	5.4 (4.6)	16 (22)

[a] Value before brackets is the average bulk composition between the etching time of 0 and 270 s.
[b] Value between brackets is composition at surface.

Table 3
Analysis of N 1s XP spectra of Si substrate before and after PA-ALD of TiO_xN_{2-x} layers.

Recipe	Plasma exposure time (s)	Fraction (%) $N_{interst}$	Fraction (%) N_{subst}	Total N surface content (at%)
–	–	–	–	0.0
O_2	2	100	–	0.3
	5	100	–	0.3
	15	100	–	0.7
	20	80	20	1.1
N_2	5	50	50	11
Combined	10	95	5	5.4

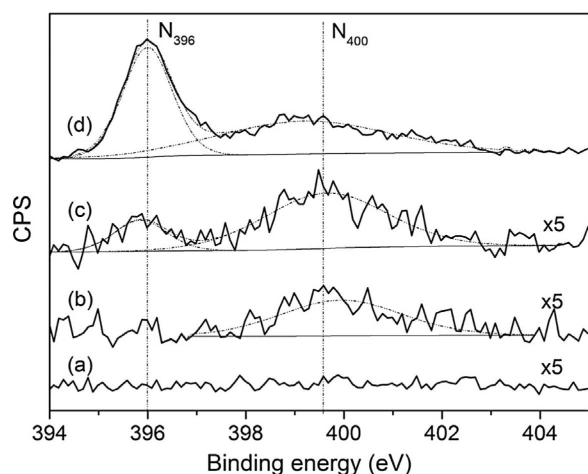

Fig. 3. Surface N 1s XP spectra of (a) pristine Si wafer and $TiO_{2-x}N_x$ thin layer prepared by PA-ALD on Si wafers using the O_2 recipe with plasma times of (b) 5 s, (c) 20 s, and (d) the N_2 recipe with plasma time of 5 s.

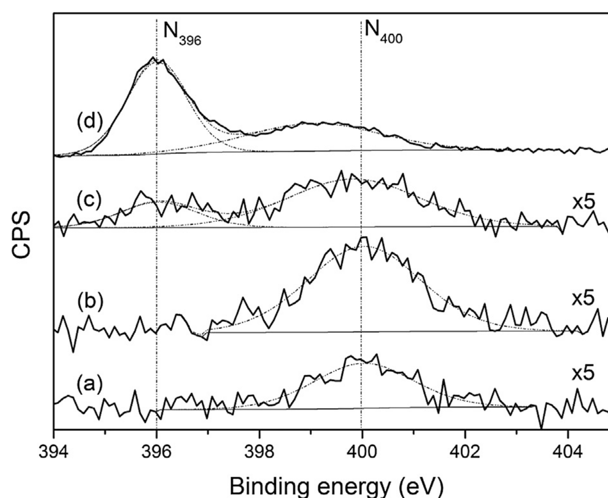

Fig. 4. Surface N 1s XP spectra of (a) pristine calcined Ti foil and $TiO_{2-x}N_x$ thin layers prepared by PA-ALD on calcined Ti foils using the O_2 recipe with different plasma time of (b) 5 s, (e) 20 s, and (d) the N_2 recipe with plasma time of 5 s.

possible locations for the N atom in the interstices of TiO_2 and found its most stable site to be in coordination to one lattice O anion. The species with N 1s binding energy of 396 eV is usually ascribed to substitutional N (N_{subst}). It implies the formation of Ti–N bonds with a covalent character, which is usually argued to be accompanied by reduction of Ti^{4+} to Ti^{3+} [22,53].

3.2. PA-ALD on calcined Ti foils

As the films are very thin, XRD patterns of the calcined Ti foil prior and after the PA-ALD process only show diffraction peaks of Ti metal (Fig. S1 in Supplementary Information). From XPS depth profiling the thickness of the TiO_2 layer of the calcined starting foil was estimated to be 36 nm. Table 2 contains the thickness of the layer deposited on the starting foils by PA-ALD and their composition obtained by XPS depth profiling. The corresponding depth profiles are given in Fig. S2. It is seen that the calcined Ti foil already contains a small amount of N. The thickness of the PA-ALD layer deposited by the O_2 recipe is estimated to be 18 nm on the basis of the etching time and assuming that the density of this PA-ALD layer is similar to the one deposited for the TiO_2 layer on the Si wafer. In the same way, the thickness of the layers deposited by the N_2 and combined recipes are 16 and 18 nm, respectively.

Fig. 4 shows N 1s XP spectra of the various foils prior and after the PA-ALD treatment. The results of the deconvolution of the N 1s peak are collected in Table 4. It is observed that for deposition using the O_2 recipe with plasma times between 2 and 10 s, only $N_{interst}$ is present. When the plasma exposure time increased to 20 s, a small additional small feature of N_{subst} is observed in the XP spectrum. This trend is consistent with the PA-ALD series for the Si substrate. For the N_2 and combined recipes, the N_{subst} feature dominates the N 1s XP spectra. For the N_2 recipe, the surface N content is seen to increase with increasing plasma exposure time (7.4 at% for 5 s and 12.8 at% for 15 s), showing that the N content can be tuned by varying the plasma exposure time in N_2 atmosphere. The surface N content is higher than that found for the layers obtained by the O_2 recipe. Consistent with the results for the Si substrate, the combined recipe gives intermediate N content, again with predominantly N_{subst} at the surface. Thus, the trends in the N content for the various PA-ALD recipes are qualitatively similar for the Si wafer and the calcined Ti foil, although careful comparison shows that for the N_2 and mixed recipes less N is incorporated for the Ti foil and, also, lower $N_{interst}/N_{total}$ ratios are found when compared to the Si wafer.

Fig. 5 and Table 5 report specific information on the composition of the layer as a function of the thickness/etching time for several recipes. For the pristine calcined Ti foil and the O_2 recipe with plasma time of 10 s the N content remains below 1 at% throughout the film. It is seen that the dominant N species at the surface is of the interstitial type while deeper into the film a small amount of N_{subst} appears. For the N_2 (plasma time 5 s) and the combined recipe (plasma time 10 s) the N content below the surface decreases stronger and similar to the above observations there is less $N_{interst}$ and more N_{subst}. It is also seen that there is carbon in all the layers, decreasing in amount deeper into the film.

Photocurrent densities of these Ti foil derived materials are shown in Fig. S3. The stable photocurrents under visible light illumination are given in Table 4. The photocurrent of the calcined Ti foil is 9 $\mu A/cm^2$. Deposition of a thin layer using the O_2 recipe with a plasma exposure time of 2 s does not result in an increase of the photocurrent, consistent with the nearly similar amount of $N_{interst}$. Increasing plasma exposure time to 5 and 10 s results in a significant increase of the photocurrent density to 15 and 18 $\mu A/cm^2$, respectively. This increase correlates well with the increase in the amount of $N_{interst}$. A plasma exposure time of 20 s results in a strong decrease of the photocurrent density to 5 $\mu A/cm^2$. Table 4 shows that the N content is similar to the one in the layers prepared at plasma exposure times of 5 and 10 s. The longer exposure time has led to the formation of N_{subst}, which has before been reported as detrimental to current evolution [28]. Consistent with this, Table 4 shows that the much higher amounts of N_{subst} in the films prepared by PA-ALD with the N_2 and combined recipes results in very low photocurrent densities.

According to earlier studies [23,28,31,55], $N_{interst}$ contributes to formation of impurity levels above the valence band of TiO_2 by hybridization of O 2p state. Therefore, the photo-induced excitation of electrons from these impurity levels towards the conduction band of TiO_2 becomes favourable. Thus, the presence of $N_{interst}$ improves the photocurrent. On the other hand, the presence of N_{subst} causes a decrease of the photocurrent, because substitution of an O atom by an N atom produces a Ti^{3+}, which can act as electron-hole recombination center. Therefore, we conclude that the influence of the titania film composition in terms of $N_{interst}$ and N_{subst} content in PA-ALD $TiO_{2-x}N_x/TiO_2/Ti$ foil on the photocurrent density is qualitatively similar to what we have discussed earlier [28]. Chen et al. have reported that N_2 plasma treatment of TiO_2 results in N doping and increased photocatalytic

Table 4
Nitrogen content and configuration and photocurrent density of ultra-thin $TiO_{2-x}N_x$ layers on the calcined Ti foil substrate by PA-ALD.

Recipe	Plasma exposure time (s)	Fraction (%) $N_{interst}$	Fraction (%) N_{subst}	Total N surface content (at%)	Photocurrent density ($\mu A/cm^2$)
–	–	100	0	0.7 ± 0.2	9 ± 2
O_2	2	100	0	0.8 ± 0.2	9 ± 1
	5	100	0	1.3 ± 0.7	15 ± 6
	10	100	0	1.1 ± 0.4	18 ± 4
	20	76	24	1.1 ± 0.2	5 ± 1
N_2	5	39	61	7.4 ± 0.5	2 ± 1
	15	27	73	13 ± 0.6	1 ± 1
Combined	10	29	71	4.6 ± 1.1	1 ± 1

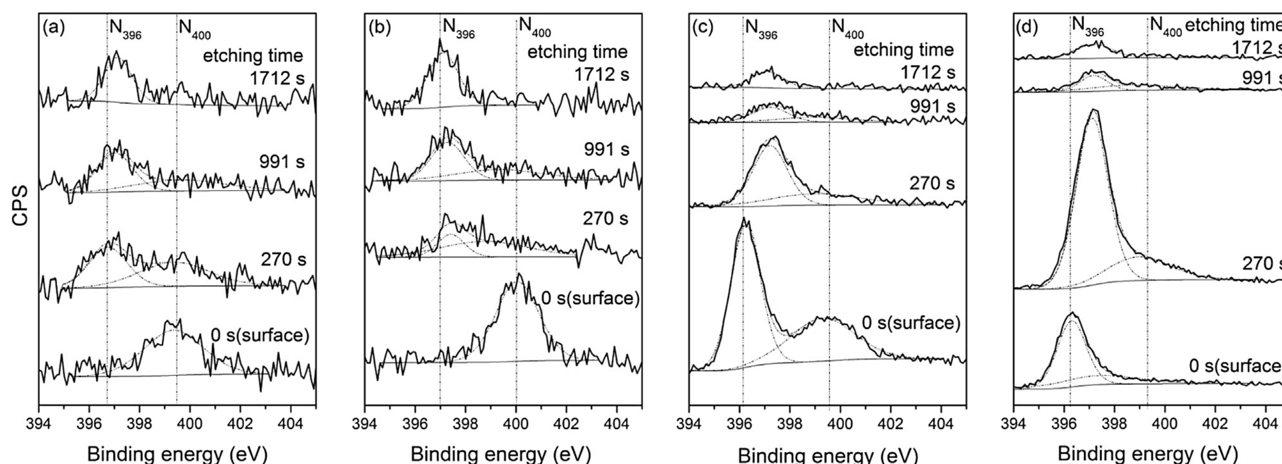

Fig. 5. N 1s XP spectra as a function of depth of (a) pristine calcined Ti foil and (b–d) $TiO_{2-x}N_x$ thin layers prepared by PA-ALD on calcined Ti foils using the (b) O_2 recipe with plasma time of 10 s, (c) N_2 recipe with plasma time of 5 s, and (d) the combined recipe with plasma time of 10 s.

activity towards isopropyl alcohol decomposition [56], although these authors did not provide clear evidence about the nature of the N species that affect photocatalytic activity. Romero-Gomez et al. prepared N-containing TiO_2 thin films by plasma enhanced (PE)-CVD and reported about formation of $N_{interst}$ species with a binding energy around 400 eV (assigned as Ti–NO species) for low N content and Ti–N (N_{subst}) for high N content [57]. They reported that N_{subst} species contribute to band gap narrowing, whereas the $N_{interst}$ species have no effect on the band gap. Also in the study of Romero-Gomez et al., no photocatalytic activities were determined.

In view of our earlier results on nitridation by thermal treatment in NH_3, the calcined Ti foils were also treated by NH_3 at 500 and 600 °C, respectively. The N 1s XP spectra of the pristine and NH_3-treated foils are shown in Fig. S4. The N content of the calcined Ti foil is 0.5 at%. It increases to 3.2 and 15.1 at% after calcination in NH_3 at 500 and 600 °C, respectively. The N 1s spectra show that the calcined foil only contains $N_{interst}$, whereas the films were found to contain also N_{subst} after NH_3 treatment. The N 1s peak at 398 eV is ascribed to N–Ti–O species [58]. Such state was also observed in NH_3-treated TiO_2 nanotubes after nitridation above 525 °C [28]. The fraction of N_{subst} increases from ca. 11 at% after NH_3 treatment at 500 °C to 48 at% after NH_3 treatment at 600 °C. Together with the increase of the N_{subst} content the Ti $2p_{3/2}$ feature is seen to shift to lower binding energy, indicative of the formation of Ti^{3+} [28,52]. Compared to the calcined foil (9 $\mu A/cm^2$), the photocurrent densities of the films are 1 and ~0 $\mu A/cm^2$ after NH_3 treatment at 500 and 600 °C, respectively. This is caused by the high N_{subst} content and the presence of associated Ti^{3+} centers, which are known to act

Table 5
Nitrogen content and configuration as a function of depth of ultra-thin $TiO_{2-x}N_x$ layers on the calcined Ti foil substrate by PA-ALD.

Recipe	Plasma exposure time (s)	Etching time (s)	Film composition (at%)			
			Ti	O	N	C
Pristine	–	0	20	60	0.7	19
		270	31	61	1.1	6.5
		991	48	43	0.6	–
		1712				8.5
O_2	10	0	18	67	1.1	14
		270	32	66	0.7	1.4
		991	35	61	0.8	3.2
		1712	49	43	0.8	7.1
N_2	5	0	11	33	7.4	49
		270	32	62	3.0	3.1
		991	36	59	1.0	3.9
		1712	54	37	0.8	8.0
Combined	10	0	22	49	4.6	24
		270	–	–	–	–
		991	34	61	1.5	3.5
		1712	40	50	1.2	8.7

as recombination centers [22,53]. Earlier, we have established that NH_3 treatment of nanotubular TiO_2 arrays at 500 °C only resulted in $N_{interst}$ and increased the photocurrent density as compared to the pristine nanotubes. These results indicate that the surface chemical properties of the nanotubular TiO_2 arrays and the TiO_2 on the calcined Ti foil are different.

3.3. PA-ALD on nanotubular TiO_2 arrays

XRD patterns of the nanotubular TiO_2 arrays prior and after PA-ALD are shown in Fig. S5. The pristine nanotubular TiO_2 arrays have the anatase structure. The PA-ALD treatment has no effect on this structure. The SEM images in Fig. 6 show the vertically aligned nanotubular TiO_2 arrays with their open tip and closed bottom structures. Fig. 6 (a) specifically shows the top of the surface of the arrays. It allows estimating the inner and outer diameters of the nanotubes to be 85 and 100 nm, respectively. The inset in Fig. 6 (a) shows that the length of the pristine nanotubular TiO_2 arrays is longer than 1 μm. The surface view by SEM nanotubular TiO_2 arrays after PA-ALD using the O_2 recipe with plasma exposure time of 10 s is given in Fig. 6 (c). It shows that a layer has been deposited on its surface as the inner and outer diameters are 35 and 120 nm, respectively. It is difficult to estimate the length of the tubes from these images, as they seem to be broken in the middle (see insert Fig. 6 (c)). Fig. 6 (e) shows the inner and outer diameters of nanotubular TiO_2 arrays after PA-ALD using the O_2 recipe with longer plasma exposure time (20 s). The morphology of this sample is very similar to the sample obtained using a plasma exposure time of 10 s. The SEM images clearly demonstrate that the surface morphology is affected by the PA-ALD processing. The deposition of a layer has resulted in much smaller pores of the nanotubes. It is expected that the plasma exposure time hardly affects the nanotube wall thickness, as this latter is controlled by the number of the ALD cycles. With the same number of PA-ALD cycles, the GPC of $TiO_{2-x}N_x$ thin layer on the open part of the nanotubular TiO_2 arrays is similar to the one of the calcined Ti foil, based on the deposited thickness

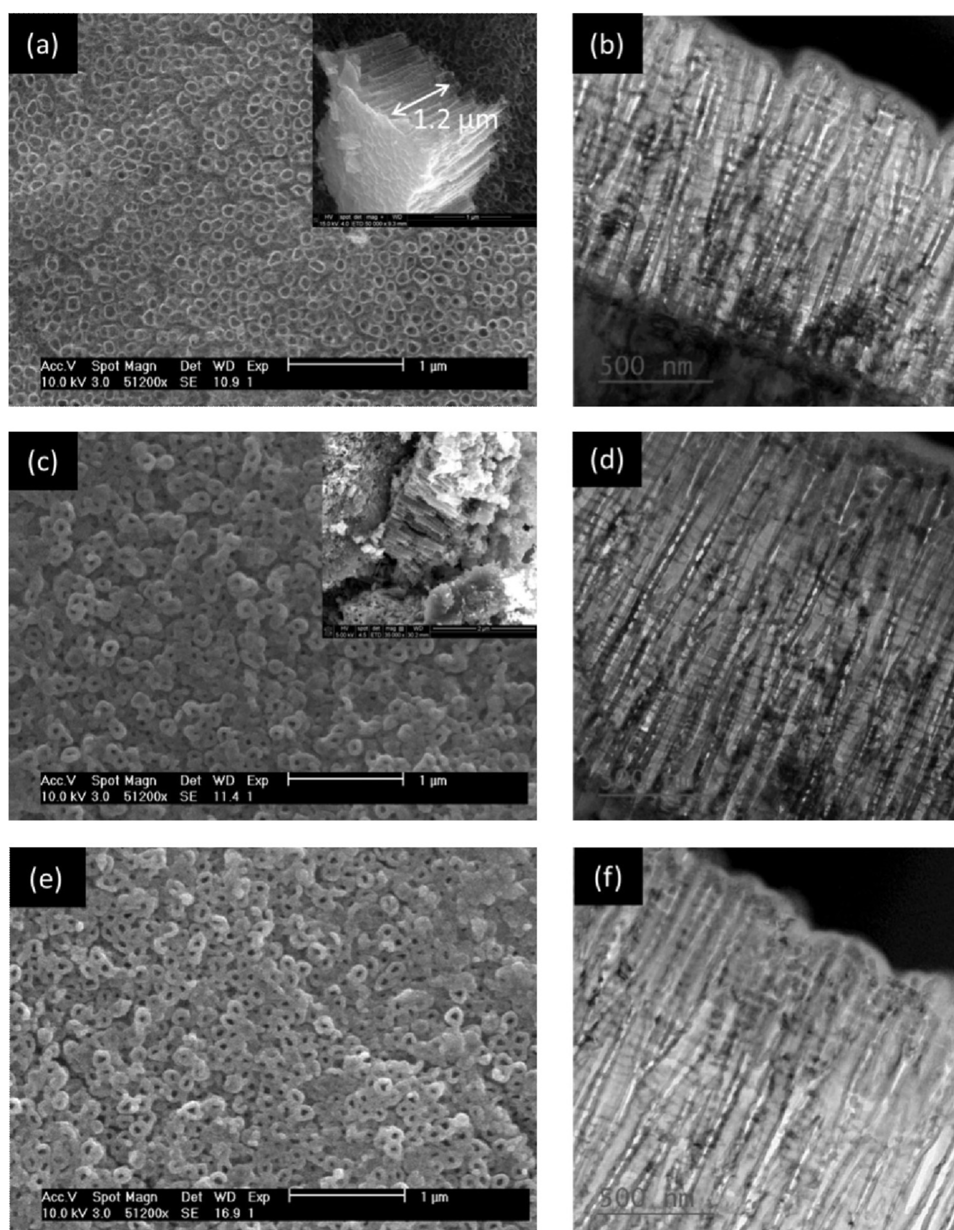

Fig. 6. SEM (a, c and e) and TEM images (b, d and f): (a and b) pristine nanotubular TiO_2 arrays, and (c and d) $TiO_{2-x}N_x$ thin layer prepared by PA-ALD on nanotubular TiO_2 arrays using the O_2 recipe with short plasma time (plasma time of 10 s) and (e and f) longer plasma time (plasma time of 20 s).

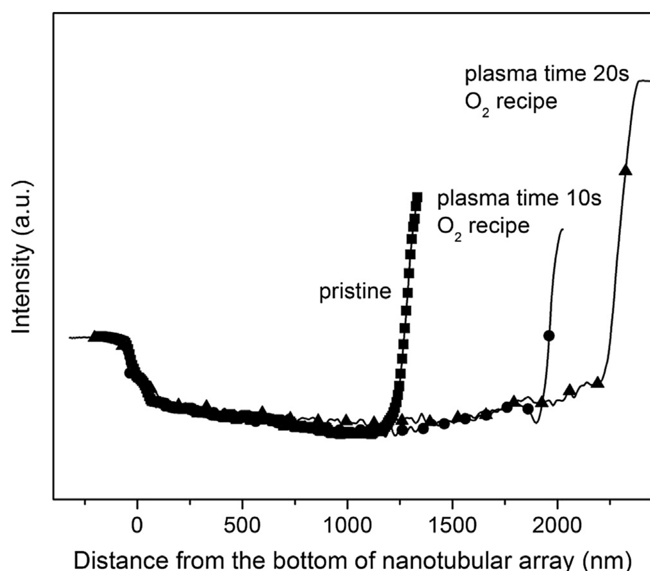

Fig. 7. Material density of pristine nanotubular TiO_2 arrays and $TiO_{2\text{-}x}N_x$ thin layer prepared by PA-ALD on nanotubular TiO_2 arrays using O_2 recipe with short plasma time (plasma time of 10 s) and longer plasma time (plasma time of 20 s).

on the outer wall of the NTs. It should be noticed that the GPC will be influenced by the roughness of the nanotube wall, which is expected to vary for individual nanotube samples.

The bright field TEM images in Fig. 6 (b), (d) and (f) show corresponding cross-sectional views of the three samples shown in Fig. 6 (a), (b) and (c), respectively. The white areas represent porosity in between the nanotubes. The TEM sample thickness is of the same order of magnitude as the distance between the tubes. The TEM image is a projection of all features within the slice of material, implying overlap of features. As a result, not all pores appear clearly in the image. The contrast in these images has several contributions, namely (i) diffraction contrast, in this case TiO_x crystals present in strongly diffracting orientations will look black in the image, (ii) materials density contrast, providing different grey scales for the different materials, and (iii) reduction in brightness if more material is present, *i.e.* in case a pore is partly filled. The latter can be observed by the variation in average grey-level in the vertical direction. The darker grey 'layer' close to the surface points to the deposition of the $TiO_{2\text{-}x}N_x$ thin layer in the upper part of the nanotubular arrays. The lighter part beneath it represents areas with a thinner PA-ALD $TiO_{2\text{-}x}N_x$ layer. Fig. 7 visualizes the brightness profiles in the TEM images along the nanotube length. It clearly shows reduced brightness close to the surface of the plasma-treated samples, pointing out the deposition effect of the ALD processes. The length of pristine nanotubular TiO_2 is 1.2–2 μm, consistent with the data shown in Fig. 6 (a). The shorter length of the pristine nanotubular TiO_2 arrays as compared to the treated samples is a consequence of the difficulty in reproducing nanotubular arrays of similar length.

Fig. 8 shows the N 1s XP spectra of the nanotubular TiO_2 arrays before and after PA-ALD. After PA-ALD with the O_2 recipe, a small feature around 400 eV due to $N_{interst}$ is observed. The surface N content is not higher than that in the pristine material. It is also seen that the N content and the N configuration do not change with variation in plasma exposure time. In contrast, after PA-ALD with the N_2 and combined recipes, substantial amounts of $N_{interst}$ and N_{subst} are seen in the XP spectra. The composition of the surface of the $TiO_{2\text{-}x}N_x$ layers deposited on nanotubular TiO_2 arrays using different recipes and plasma exposure times are listed in Table 6.

The photocurrent densities of these films are reported in Table 6 and Fig. 9. Several important observations can be made. The photocurrent density of the pristine nanotubular TiO_2 arrays is much

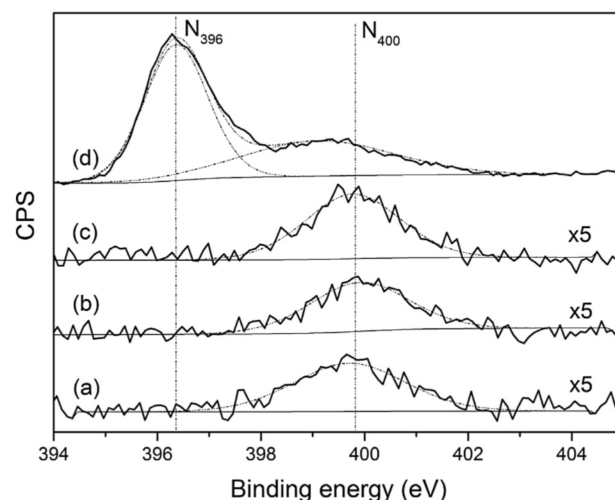

Fig. 8. Surface N 1s XP spectra of (a) pristine and $TiO_{2\text{-}x}N_x$ thin layers prepared by PA-ALD on nanotubular TiO_2 arrays using the O_2 recipe with plasma time of (b) 2 s, (c) 20 s, and using the N_2 recipe with plasma time of (d) 5 s.

higher than that of the thin conformal layers deposited on calcined Ti foil substrates. As mentioned earlier, nanotubular arrays possess higher surface area and facilitate charge transfer at the solid/liquid junction [17,18]. Furthermore, the photocurrent density does not depend strongly on the plasma exposure time for the O_2 recipe as compared to its influence determined for the TiO_2 calcined foil. The N content does not increase with respect to the pristine NT composition and stays below 1 at%. These appear to be the main reasons for the nearly constant and comparable to the pristine sample photocurrent density. Furthermore, in agreement with the earlier observation on the effect of substantial amounts of N_{subst} in the layer using the N_2 and combined recipes, we confirm that N_{subst} results in a strong decrease of the photocurrent.

We should also point out that the photocurrent densities of the pristine TiO_2 nanotubular arrays in the present study differ from the one reported in our earlier publication [28]. Besides variations from batch to batch in nanotube synthesis, the slightly different equipment used for anodization and calcination, especially the use of different lamps for the photoelectrochemical characterization (a Xe lamp was used in earlier work [28] *vs.* the Hg + Xe lamp in the present study) is expected to contribute to the different

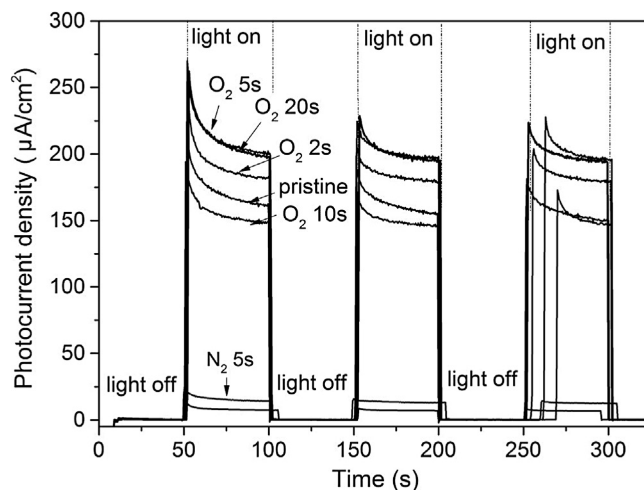

Fig. 9. Photocurrent density under visible light irradiation of pristine and $TiO_{2\text{-}x}N_x$ thin layers prepared by PA-ALD on nanotubular TiO_2 arrays using the O_2 recipe with plasma time of 2–20 s, the N_2 recipe with plasma time of 5 s, and the combined recipe with plasma time of 10 s.

Table 6
Nitrogen content and configuration from XPS and photocurrent density of $TiO_{2-x}N_x$ layers deposited on the nanotubular TiO_2 arrays by PA-ALD.

Recipe	Plasma exposure time (s)	Fraction $N_{interst}$ (%)	Fraction N_{subst} (%)	Total N surface content (at%)	Photocurrent density ($\mu A/cm^2$)
–	–	100	0	0.8 ± 0.5	190 ± 14
O_2	2	100	0	0.6 ± 0.2	180 ± 4
	5	100	0	0.9 ± 0.5	200 ± 30
	10	100	0	0.7 ± 0.4	150 ± 14
	20	100	0	0.4 ± 0.3	180 ± 30
N_2	5	39	61	7.4 ± 0.5	10
Combined	10	29	71	4.6 ± 1.1	6

photocurrent densities. Although in all measurements the output power of the lamp was set to 300 W, the irradiation energy density below 500 nm was found to be very different. The energy in the 420–630 nm wavelength range of the Hg + Xe lamp is much higher than that of the Xe lamp. This is the main reason why the photocurrent densities in our present work are substantially higher than those in our previous work.

4. General discussion

The present study focuses on the impact of thin $TiO_{2-x}N_x$ layers in terms of N content, N oxidation state and homogeneity in PA-ALD treatment, when deposited on calcined Ti foil and NT TiO_2, with the final aim of improving their photocatalytic performance. As our previous study [28] as well as other literature studies [22] pointed out the beneficial role of $N_{interst}$ on the photocurrent, the extent of N-doping and the N state in the PA-ALD layers have been characterized. Initially, layers deposited on Si wafer reference substrates were characterized. By varying the background gas injected through the ICP dosing line and the plasma exposure time, it is possible to control to some extent the N content in the deposited $TiO_{2-x}N_x$ thin layer. The use of O_2 as background gas results in very low N content in the deposited film (1.1 at% for 20 s plasma exposure). The use of N_2 results in $TiO_{2-x}N_x$ layers with N content above 11 at%. Intermediate N content can be achieved by alternating cycles using O_2 and N_2 gases. It is noticed that the N_2 recipe leads to $TiO_{2-x}N_x$ instead of TiN because of sample oxidation upon exposure to the ambient.

Next to the relative N content, this study has focused on the oxidation state of N. Typically, two N 1s states are observed. The one with a binding energy around 400 eV is attributed to $N_{interst}$ and the other one with binding energy around 396 eV corresponds to N_{subst}. For the O_2 recipe, it is found that the N content has always an interstitial character up to a plasma exposure time of 10 s, while for longer plasma times as well as in the case of the N_2 and combined recipes, a contribution of N_{subst} appears in the XP spectra (see Table 3).

The three deposition recipes were then first employed to deposit a conformal $TiO_{2-x}N_x$ layer on a planar TiO_2 substrate, *i.e.* a calcined Ti foil. The composition of the deposited layers is found very similar to the one of the layers deposited on Si substrate. Note an initial N content of 0.8 at% (0.7 at% at the surface) was detected in the pristine calcined Ti foil. The $TiO_{2-x}N_x/TiO_2/Ti$ substrates were evaluated for their photoelectrochemical response using visible light. Introduction of $N_{interst}$ using the O_2 recipe improved the photocurrent density. The increase in photocurrent density correlated with the amount of $N_{interst}$, *i.e.* an improvement from 9 to 18 $\mu A/cm^2$ was observed for a plasma exposure time of 10 s corresponding to 1.1 at% N content. These results are consistent with parallel literature studies, where PA-ALD and thermal ALD of N-doped TiO_2 were investigated: a concentration of N around 1 at% exhibiting a major contribution of 400 eV is responsible for more efficient degradation of methylene blue [59,60]; a higher N concentration inevitably leads to a high defect concentration decreasing the photo-activity [61]. Consistent with our previous work [28], the photocurrent density strongly decreased when N_{subst} was present. Accordingly, all substrates prepared by PA-ALD using the N_2 or combined recipe exhibited negligible photoresponse.

The same PA-ALD recipes were applied for the deposition of $TiO_{2-x}N_x$ layers on nanotubular TiO_2 arrays. All PA-ALD processes result in an inhomogeneous layer along the length of the NTs. SEM images point out based on the changes of the NT outer diameter, a growth per cycle similar to the cases of Si and calcined Ti foil substrates. TEM analysis of cross-sections perpendicular to the nanotube length axes reveals that the deposition has mainly occurred along the top part of the nanotubes; the bottom of the tubes appears hardly affected. There are several reasons for a lack of homogeneity in the PA-ALD process. One of them is the mass transfer limitation of the bulk Ti precursor along the length of the NT [62,63]. Adsorption processes are also of key importance of a conformal film growth: the Ti precursor adopted in this study has been subject of investigation of DFT calculations summarized in [64], demonstrating that its adsorption at the surface is favourable only when occurring from the side of the amino-ligands, due to their polarity (with respect to the Cp ligand) and therefore affinity with OH-terminated surfaces. Furthermore, the same calculations have shown that, differently from the classical scheme of ALD surface reactions, there is lack of full condensation reaction between the Ti precursor and the OH-terminated surface, *i.e.* no direct bond occurs with the surface O accompanied by loss of one or more Me_2NH molecules, due to steric crowding and reduced electrophilicity imposed by the Cp ligand on the Ti centre. This is also the main reason why this precursor does not lead to TiO_2 deposition when a thermal ALD process is setup (*i.e.* in the presence of H_2O) but only when plasma is applied. Therefore, we conclude that if the surface of the internal and external walls of the NTs is not homogeneous in terms of OH-termination, this would lead to a heterogeneous deposition process. Furthermore, plasma activation is essential in promoting film growth because it induces surface reactivity in the form of carbon removal and insertion of OH groups for the subsequent Ti precursor exposure and adsorption. However, the radicals produced in a H_2/N_2-fed plasma (*e.g.* N, H, NH, NH_2) exhibit a high reactivity in terms of functionalization of the surface as well as carbon removal in the form of HCN [65] and such reactivity is not compatible with a long radical diffusion path/long life time along the NT length necessary to deliver a conformal deposition.

In terms of film composition, similar observations to the cases of Si and calcined Ti foil substrates can be drawn: the N content is found to be the lowest for the O_2 recipe and highest for the N_2 recipe. Also, the incorporated N is always present in the interstitial state and substitutional N develops only for the N_2 and combined recipes. However, the N content of the layers deposited by the O_2 recipe hardly varies with the plasma exposure time and it is always below 1 at%. Furthermore, also the N_2 and combined recipes deliver lower N concentration when compared to the depositions on Si and calcined Ti foil. Finally, the N content in the pristine TiO_2 NTs is higher than in the other pristine substrates, *i.e.* 0.8 at%. As already pointed out during the discussion on the NH_3 treatment,

the nitridation process on calcined TiO_2 and TiO_2 NTs had led to different results in terms of N content and N oxidation state. This was attributed to the different surface properties of the two substrates, which can definitely apply also to the case of the PA-ALD process here under investigation. As earlier mentioned, the surface properties of substrate seriously affect the adsorption of the Ti precursor.

The photocurrent density of the pristine TiO_2 NTs is about 20 times higher than the one of calcined TiO_2, which is due to its higher surface area. Given the absorption coefficient of titania [66], light absorption will take place at the top 1 μm along the length axis of the nanotubes. After PA-ALD processing with the O_2 recipe, there is no noticeable change in the photocurrent density, which we relate to the fact that, under the O_2 recipe, no additional N-doping takes place, given the relatively high N concentration present already in the pristine NTs. The detrimental effect of N_{subst} is once again experienced, as in the case of the NTs treated according to the N_2 or the combined recipe, where a strong decrease in photocurrent is observed, from 190 down to 10 $\mu A/cm^2$. It is worthy of note that, although the relative N content as well as of N_{subst} content are similar in both N_2 and combined recipes carried out on bulk TiO_2 and TiO_2 NTs, only the latter are characterized by a massive reduction of current density, while the current density for the former decreases just of a factor 4. This is to be attributed to the increased surface area in the case of the NTs. This result further suggests that, although the PA-ALD process does not lead to a homogeneous growth along the whole length of the NT, the extent of the treatment along the length of the NT (*i.e.* approx. 1/3 of the length of the NT) is sufficient to experience the detrimental effect of the incorporation of N_{subst} on the photocurrent. In comparison, literature has shown that it is possible to develop a uniform and conformal ultra-thin N-containing carbon layer on the walls of TiO_2 NTs by means of molecular layer deposition (MLD) of PMDA/EDA, leading to an increase in photocurrent density of factor 5 with respect to the pristine NTs [67].

5. Conclusions

To develop a PA-ALD procedure for N doping on calcined TiO_2 and nanotubular TiO_2 arrays, $TiO_{2-x}N_x$ layers were first deposited and characterized in terms of N content and oxidation state on Si wafers. Two characteristic N 1s peaks are observed at 400 and 396 eV, which are ascribed to interstitial and substitutional N doping ($N_{interst}$ and N_{subst}). The $N_{interst}$ doping is dominant when O_2 flow is used as background gas (lower N content) and N_{subst} is dominant when the N_2 recipe is used, combined recipe as well as using O_2 recipe with longer plasma time (20 s). In the case of the O_2 recipe, the photocurrent density of the calcined Ti foil upon PA-ALD treatment increases of a factor 2 with respect to the pristine foil, for a plasma exposure time up to 5–10 s. When the N_2 recipe is used, the photocurrent density decreases. The enhancement in photocurrent density of calcined Ti foil after PA-ALD is ascribed to $N_{interst}$ which develop when the O_2 recipe is adopted. In the case of the N_2 recipe, an increased N content leads to the development of N_{subst}, detrimental to the photocurrent density.

The nanotubular TiO_2 arrays exhibit a photocurrent density about 20 times higher than the one of calcined TiO_2, due to the increased surface area. When modified by a PA-ALD deposited $TiO_{2-x}N_x$ thin layer no improvement in terms of photocurrent density is observed, regardless the plasma exposure time under the O_2 recipe condition. This is attributed to the fact that no additional N-doping occurs, given the relatively high N concentration present already in the pristine NTs. TEM analysis of cross-sections perpendicular to the nanotube length axes reveals that the deposition has mainly occurred along the top part of the nanotubes. The bottom of the tubes appears hardly affected. The detrimental effect of N_{subst} is once again experienced, as in the case of the NTs treated according to the N_2 or the combined recipe, where a massive decrease in photocurrent is observed, from 190 down to 10 $\mu A/cm^2$. This result further suggests that, although the PA-ALD process does not lead to an homogeneous growth along the whole length of the NT, the extent of the treatment along the length of the NT (*i.e.* approx. 1/3 of the length of the NT) is sufficient to experience any beneficial or detrimental effect of the PA-ALD treatment, *e.g.* in this case the effect of the incorporation of N_{subst} on the photocurrent.

Acknowledgements

The authors gratefully acknowledge the financial support of this work by the Royal Netherlands Academy of Sciences and Arts and the Chinese Ministry of Science and Technology. The research was mainly carried out in the Inorganic Materials Chemistry in Eindhoven University of Technology (TU/e) as a part of the collaboration Programme Strategic Scientific Alliances (PSA). The PA-ALD processing was carried out in the cleanroom at NanoLab@TU/e. The authors thank Valentino Longo for the experimental support and the useful discussions on the PA-ALD processing. The research of M.C. has been funded by the Netherlands Organization for Scientific Research (NWO, Aspasia program).

References

[1] A.L. Linsebigler, G. Lu, J.T. Yates Jr., Photocatalysis on TiO_2 surfaces: principles, mechanisms, and selected results, Chem. Rev. 95 (1995) 735–758.
[2] F. Wen, J. Yang, X. Zong, Y. Ma, Q. Xu, B. Ma, C. Li, Photocatalytic hydrogen production utilizing solar energy, Prog. Chem. 21 (2009) 2285–2302.
[3] W. Choi, A. Termin, M.R. Hoffmann, The role of metal ion dopants in quantum-sized TiO_2: correlation between photoreactivity and charge carrier recombination dynamics, J. Phys. Chem. 98 (1994) 13669–13679.
[4] H. Yamashita, M. Honda, M. Harada, Y. Ichihashi, M. Anpo, Preparation of titanium oxide photocatalysts anchored on porous silica glass by a metal ion-implantation method and their photocatalytic reactivities for the degradation of 2-propanol diluted in water, J. Phys. Chem. B 102 (1998) 10707–10711.
[5] Y. Wang, H. Cheng, Y. Hao, J. Ma, W. Li, S. Cai, Photoelectrochemical properties of metal-ion-doped TiO_2 nanocrystalline electrodes, Thin Solid Films 349 (1999) 120–125.
[6] R. Asahi, T. Morikawa, T. Ohwaki, K. Aoki, Y. Taga, Visible-light photocatalysis in nitrogen doped titanium oxides, Science 293 (2001) 269–271.
[7] T. Umebayashi, T. Yamaki, H. Itoh, K. Asai, Band gap narrowing of titanium dioxide by sulfur doping, Appl. Phys. Lett. 81 (2002) 454–456.
[8] J.C. Yu, J. Yu, W. Ho, Z. Jiang, L. Zhang, Effects of F^- doping on the photocatalytic activity and microstructures of nanocrystalline TiO_2 powders, Chem. Mater. 14 (2002) 3808–3816.
[9] S. Sato, Photocatalytic activity of NO_x-doped TiO_2 in the visible light region, Chem. Phys. Lett. 123 (1986) 126–128.
[10] S. Livraghi, M.C. Paganini, E. Giamello, A. Selloni, C. Di Valentin, G. Pacchioni, Origin of photoactivity of nitrogen-doped titanium dioxide under visible light, J. Am. Chem. Soc. 128 (2006) 15666–15671.
[11] M. Adachi, Y. Murata, I. Okada, S. Yoshikawa, Formation of titania nanotubes and applications for dye-sensitized solar cells, J. Electrochem. Soc. 150 (2003) G448–G493.
[12] O.K. Varghese, M. Paulose, K. Shankar, G.K. Mor, C.A. Grimes, Water-photolysis properties of micro-length-highly-ordered titania nanotube-arrays, J. Nanosci. Nanotech. 5 (2005) 1158–1165.
[13] D. Gong, C.A. Grimes, O.K. Varghese, Titanium oxide nanotube arrays prepared by anodic oxidation, J. Mater. Res. 16 (2001) 3331–3334.
[14] G.K. Mor, K. Shankar, M. Paulose, O.K. Varghese, C.A. Grimes, Use of highly-ordered TiO_2 nanotube arrays in dye-sensitized solar cells, Nano Lett. 6 (2006) 215–218.
[15] K. Shankar, G.K. Mor, H.E. Prakasam, S. Yoriya, M. Paulose, O.K. Varghese, C.A. Grimes, Highly-ordered TiO_2 nanotube arrays up to 220 μm in length: use in water photoelectrolysis and dye-sensitized solar cells, Nanotechology 18 (2007), 065707 (11pp).
[16] M. D'Arienzo, R. Scotti, L. Wahba, C. Battocchio, E. Bemporad, A. Nale, F. Morazzoni, Hydrothermal N-doped TiO_2: explaining photocatalytic properties by electronic and magnetic identification of N active sites, Appl. Catal. B: Environ. 93 (2009) 149–156.
[17] C. Burda, Y. Lou, X. Chen, A.C.S. Samia, J. Stout, J.L. Gole, Enhanced nitrogen doping in TiO_2 nanopartices, Nano Lett. 3 (2003) 1049–1051.
[18] S. Sato, R. Nakamura, S. Abe, Visible-light sensitization of TiO_2 photocatalysts by wet-method N doping, Appl. Catal. A: Gen. 284 (2005) 131–137.
[19] R. Beranek, B. Neumann, S. Sakthivel, M. Janczarek, T. Dittrich, H. Tributsch, H. Kisch, Exploring the electronic structure of nitrogen-modified TiO_2

photocatalysts through photocurrent and surface photovoltage studies, Chem. Phys. 339 (2007) 11–19.
[20] H. Kisch, S. Sakthivel, M. Janczarek, D. Mitoraj, A low-band gap, nitrogen-modified titania visible-light photocatalyst, J. Phys. Chem. C 111 (2007) 11445–11449.
[21] S. Sakthivel, H. Kisch, Photocatalytic and photoelectrochemical properties of nitrogen-doped titanium dioxide, ChemPhysChem 4 (2003) 487–490.
[22] J. Wang, D.N. Tafen, J.P. Lewis, Z. Hong, A. Manivannan, M. Zhi, M. Li, N. Wu, Origin of photocatalytic activity of nitrogen-doped TiO_2 nanobelts, J. Am. Chem. Soc. 131 (2009) 12290–12297.
[23] J. Zhang, Y. Wang, Z. Jin, Z. Wu, Z. Zhang, Visible-light photocatalytic behavior of two different N-doped TiO_2, Appl. Surf. Sci. 254 (2008) 4462–4466.
[24] H. Irie, Y. Watanabe, K. Hashimoto, Nitrogen-concentration dependence on photocatalytic activity of $TiO_{2-x}N_x$ powders, J. Phys. Chem. B 107 (2003) 5483–5486.
[25] B. Kosowska, S. Mozia, A.W. Morawski, B. Grzmil, M. Janus, K. Kalucki, The preparation of TiO_2-nitrogen doped by calcination of $TiO_2 \cdot xH_2O$ under ammonia atmosphere for visible light photocatalysis, Sol. Energy Mater. Sol. Cells 88 (2005) 269–280.
[26] O. Diwald, T.L. Thompson, T. Zubkov, E.G. Goralski, S.D. Walck, J.T. Yates Jr., Photochemical activity of nitrogen-doped rutile TiO_2 (1 1 0) in visible light, J. Phys. Chem. B 108 (2004) 6004–6008.
[27] T. Ihara, M. Miyoshi, Y. Iriyama, O. Matsumoto, S. Sugihara, Visible-light-active titanium oxide photocatalyst realized by an oxygen-deficient structure and by nitrogen doping, Appl. Catal. B: Environ. 42 (2003) 403–409.
[28] Y. Zhang, Q.-B. Ma, L. Gao, E.J.M. Hensen, Preparation and photoelectromchemical properties of nitrogen doped nanotubular TiO_2 arrays, Appl. Surf. Sci. 282 (2013) 174–180.
[29] R.P. Vitiello, J.M. Macak, A. Ghicov, H. Tsuchiya, L.F.P. Dick, P. Schmuki, N-doping of anodic TiO_2 nanotubes using heat treatment in ammonia, Electrochem. Commun. 8 (2006) 544–548.
[30] A. Braun, K.K. Akurati, G. Fortunato, F.A. Reifler, A. Ritter, A.S. Harvey, A. Vital, T. Graule, Nitrogen doping of TiO_2 photocatalyst forms a second e_g state in the oxygen(1s) NEXAFS pre-edge, J. Phys. Chem. C 114 (2010) 516–519.
[31] A. Kafizas, C. Crick, I.P. Parkin, The combinatorial atmospheric pressure chemical vapour deposition (cAPCVD) of a gradating substitutional/interstitial N-doped anatase TiO_2 thin-film; UVA and visible light photocatalytic activities, J. Photochem. Photobiol. A: Chem. 216 (2010) 156–166.
[32] H.M. Yates, M.G. Nolan, D.W. Sheel, M.E. Pemble, The role of nitrogen doping on the development of visible light-induced photocatalytic activity in thin TiO_2 films grown on glass by chemical vapour deposition, J. Photochem. Photobiol. A: Chem. 179 (2006) 213–223.
[33] H. Natsuhara, K. Matsumoto, N. Yoshida, T. Itoh, S. Nonomura, M. Fukawa, K. Sato, TiO_2 thin films as protective material for transparent-conducting oxides used in Si thin film solar cells, Sol. Energy Mater. Sol. Cells 90 (2006) 2867–2880.
[34] B. Liu, L. Wen, X. Zhao, The structure and photocatalytic studies of N-doped TiO_2 films prepared by radio frequency reactive magnetron sputtering, Sol. Energy Mater. Sol. Cells 92 (2008) 1–10.
[35] A.L.J. Pereira, P.N. Lisboa Filho, J. Acuna, I.S. Brandt, A.A. Pasa, Enhancement of optical absorption by modulation of the oxygen flow of TiO_2 films deposited by reactive sputtering, J. Appl. Phys. 111 (2012) 1–7, 113513.
[36] S. Takeda, S. Suzuki, H. Odaka, H. Hosono, Photocatalytic TiO_2 thin film deposited onto glass by DC magnetron sputtering, Thin Solid Films 392 (2001) 338–344.
[37] Y. Suda, H. Kawasaki, T. Ueda, T. Ohshima, Preparation of high quality nitrogen doped TiO_2 thin film as a photocatalyst using a pulsed laser deposition method, Thin Solid Films 453-454 (2004) 162–166.
[38] V. Pore, A. Rahtu, M. Leskela, M. Ritala, T. Sajavaara, J. Keinonen, Atomic layer deposition of photocatalytic TiO_2 thin films from titanium tetramethoxide and water, Chem. Vap. Deposition 10 (2004) 143–148.
[39] V. Pore, M. Heikkila, M. Ritala, M. Leskela, S. Areva, Atomic layer deposition of $TiO_{2-x}N_x$ thin films for photocatalytic applications, J. Photochem. Photobiol. A: Chem. 177 (2006) 68–75.
[40] M. Heikkila, E. Puukilainen, M. Ritala, M. Leskela, Effect of thickness of ALD grown TiO_2 films on photoelectrocatalysis, J. Photochem. Photobiol. A: Chem. 204 (2009) 200–208.
[41] H.B. Profijt, S.E. Potts, M.C.M. van de Sanden, W.M.M. Kessels, Plasama-assisted atomic layer deposition: basics, opportunities, and challenges, J. Vac. Sci. Technol. A 29 (2011) 1–26, 050801.
[42] H. Kim, Atomic layer deposition of metal and nitride thin films: current research efforts and applications for semiconductor device processing, J. Vac. Sci. Technol. B 21 (2003) 2231–2261.
[43] H.B. Profijt, PhD Dissertation, Plasma-surface Interaction in Plasma-assisted Atomic Layer Deposition, Eindhoven University of Technology, Eindhoven, 2008, pp. 34–35.
[44] S.E. Potts, W. Keuning, E. Langereis, G. Dingemans, M.C.M. van de Sanden, W.M.M. Kessels, Low temperature plasma-enhanced atomic layer deposition of metal oxide thin films, J. Electrochem. Soc. 157 (2010) 66–74.
[45] H.B. Profijt, M.C.M. van de Sanden, W.M.M. Kessels, Substrate biasing during plasma-assisted ALD for crystalline phase-control of TiO_2 thin films, Electrochem. Solid-State Lett. 15 (2012) G1–G3.
[46] A. Sarkar, S.E. Potts, S.A. Rushworth, F. Roozeboom, M.C.M. van de Sanden, W.M.M. Kessels, Plasma-enhanced ALD of TiO_2 using a novel cyclopentadienyl alkylamido precursor $[Ti(Cp^{Me})(NMes)_3]$ and O_2 plasma, ECS Trans. 33 (2010) 385–393.
[47] H.B. Profijt, M.C.M. van de Sanden, W.M.M. Kessels, Substrate-biasing during plasma-assisted atomic layer deposition to tailor metal-oxide thin film growth, J. Vac. Sci. Technol. A 31 (2013) 1–9, 01A106.
[48] G.X. Liu, F.K. Shan, W.J. Lee, G.H. Lee, I.S. Kim, B.C. Shin, S.G. Yoon, C.R. Cho, Transparent titanium dioxide thin film deposited by plasma-enhanced atomic layer deposition, Integr. Ferroelectr. 81 (2006) 239–248.
[49] S.B.S Heil, E. Langereis, F. Roozeboom, M.C.M. van de Sanden, W.M.M. Kessels, J. Electrochem. Soc. 153 (2005) G956–G965.
[50] S. Deng, S.W. Verbruggen, S. Lenaerts, J.A. Martens, S. van den Berghe, K. Devloo-Casier, W. Devulder, J. Dendooven, D. Deduytsche, C. Detavernier, Controllable nitrogen doping in as deposited TiO_2 film and its effect on post deposition annealing, J. Vac. Sci. Technol. A 32 (2014) 1–7, 01A123.
[51] J.M. Macak, H. Hildebrand, U. Marten-Jahns, P. Schumki, Mechanistic aspects and growth of large diameter self-organized TiO_2 nanotubes, J. Electroanal. Chem. 621 (2008) 254–266.
[52] N.C. Saha, H.G. Tompkins, Titanium nitride oxidation chemistry: an X-ray photoelectron spectroscopy study, J. Appl. Phys. 72 (1992) 3072–3079.
[53] R. Nakamura, T. Tanaka, Y. Nakato, Mechanism for visible light responses in anodic photocurrents at N-doped TiO_2 film electrodes, J. Phys. Chem. B 108 (2004) 10617–10620.
[54] C. Di Valentin, G. Pacchioni, A. Selloni, S. Livraghi, E. Giamello, Characterization of paramagnetic species in N-doped TiO_2 powders by EPR spectroscopy and DFT calculations, J. Phys. Chem. B 109 (2005) 11414–11419.
[55] Y. Wang, C. Feng, Z. Jin, J. Zhang, J. Yang, S. Zhang, A novel N-doped TiO_2 with high visible light photocatalytic activity, J. Mol. Catal. A: Chem. 260 (2006) 1–3.
[56] C. Chen, H. Bai, C. Chang, Effect of plasma processing gas composition on the nitrogen-doping status and visible light photocatalysis of TiO_2, J. Phys. Chem. C 111 (2007) 15228–15235.
[57] P. Romero-Gomez, S. Hamad, J.C. Gonzalez, A. Barranco, J.P. Espinos, J. Cotrino, A.R. Gonzalez-Elipe, Band gap narrowing versus formation of electronic states in the gap in N-TiO_2 thin films, J. Phys. Chem. C 114 (2010) 22546–22557.
[58] B. Viswanathan, K.R. Krishanmurthy, Nitrogen incorporation in TiO_2: does it make a visible light photo-active material? Int. J. Photoenergy 2012 (2012) Article ID 269654, 10 pages.
[59] Z. Rao, J. Wan, C. Li, B. Chen, J. Liu, C. Huang, Y. Xia, In-situ nitrogen doping of the TiO_2 photocatalyst deposited by PEALD for visible light activity, Plasma Sci. Technol. 16 (2014) 239–243.
[60] M.-L. Kääriäinen, D.C. Cameron, Nitrogen doping in atomic layer deposition grown titanium dioxide films by using ammonium hydroxide, Thin Solid Films 526 (2012) 212–217.
[61] H.-E. Cheng, Y.-R. Chen, W.-T. Wu, C.-M. Hsu, Effect of nitrogen doping concentration on the properties of TiO_2 films gown by atomic layer deposition, Mater. Sci. Eng. B 176 (2011) 596–599.
[62] H.C.M. Knoops, M.E. Donders, L. Baggetto, M.C.M. van de Sanden, P.H.L. Notten, W.M.M. Kessels, Atomic layer deposition for all-solid-state 3D-integrated batteries, ECS Trans. 25 (2009) 333–344.
[63] L. Baggetto, H.C.M. Knoops, R.A.H. Niessen, W.M.M. Kessels, P.H.L. Notten, 3D negative electrode stacks for integrated all-solid-state lithium-ion microbatteries, J. Mater. Chem. 20 (2010) 3703–3708.
[64] S.E. Potts, W.M.M. Kessels, Energy-enhanced atomic layer deposition for more process and precursor versatility, Coord. Chem. Rev. 257 (2013) 3254–3270.
[65] M. Fukasawa, T. Tatsumi, K. Oshima, K. Nagahata, S. Uchida, S. Takashima, M. Hori, Y. Kamide, Surface reactions during low-*k* etching using H_2/N_2 plasma, J. Vac. Sci. Technol. A 26 (2008) 870–874.
[66] B. van der Zanden, A. Goossens, The nature of electron migration in dye-sensitized nanostructured TiO_2, J. Phys. Chem. B 104 (2000) 7171–7178.
[67] X. Tong, P. Yang, Y. Wang, Y. Qin, X. Guo, Enhanced photoelectrochemical water splitting performance of TiO_2 nanotube arrays coated with an ultrathin nitrogen-doped carbon film by molecular layer depositin, Nanoscale 6 (2014) 6692–6700.